Journal of Statistical Mechanics:
Theory and Experiment

PAPER

Effect of local dissociations in bidirectional transport of driven particles

Journal of Statistical Mechanics: Theory and Experiment
An IOP and SISSA journal

PAPER: Classical statistical mechanics, equilibrium and non-equilibrium

Effect of local dissociations in bidirectional transport of driven particles

Akriti Jindal[1], Anatoly B Kolomeisky[2] and Arvind Kumar Gupta[1,*]

[1] Department of Mathematics, Indian Institute of Technology Ropar, Rupnagar-140001, Punjab, India
[2] Department of Chemistry, Department of Chemical and Biomolecular Engineering, Department of Physics and Astronomy, Center for Theoretical Biological Physics, Rice University, Houston, TX 77005, United States of America
E-mail: akgupta@iitrpr.ac.in

Received 31 July 2020
Accepted for publication 30 September 2020
Published 9 November 2020

Online at stacks.iop.org/JSTAT/2020/113202
https://doi.org/10.1088/1742-5468/abbed7

Abstract. Motivated by the complex processes of cellular transport when different types of biological molecular motors can move in opposite directions along protein filaments while also detaching from them, we developed a theoretical model of the bidirectional motion of driven particles. It utilizes a totally asymmetric simple exclusion process framework to analyze the dynamics of particles moving in opposite directions along the lattice of discrete sites while the particles might also dissociate from the filament in the bulk of the system. Mean-field theoretical arguments supported by extensive Monte Carlo simulations are presented in order to understand how the localized particle dissociations affect the bidirectional dynamics and spontaneous symmetry-breaking phenomena. It is found that changes in the amplitudes and in the symmetry of dissociation rates lead to significant modifications in the dynamic properties and in the stationary phase diagrams. These changes are explained using simple physical arguments. Our theoretical method clarifies some aspects of microscopic mechanisms of complex transport phenomena in biological systems.

*Author to whom any correspondence should be addressed.

1742-5468/20/113202+26$33.00

Keywords: driven diffusive systems, exclusion processes, molecular motors

Contents

1. Introduction

The translocation of several classes of enzymatic molecules, known as molecular motors or motor proteins, along protein filaments inside living cells plays an important role in diverse biological processes [1–4]. These motors are the active agents that utilize chemical energy released during the hydrolysis of adenosine triphosphate for their motion along the filaments and for carrying various cellular cargoes to specific cellular compartments [1, 2, 4]. They are crucial for assembly, self-organization, functioning of cells, cell division and in the transfer of genetic information [4, 5]. These biological processes exhibit non-zero molecular fluxes, which is a signature of the non-equilibrium state of living systems.

In recent years, the mechanochemical properties of individual motor proteins have been thoroughly investigated for both *in vivo* and *in vitro* conditions using various advanced single-motor experimental techniques [4, 6, 7]. These biological motors, however, are known to function in living cells in large groups. Stimulated by the necessity

J. Stat. Mech. (2020) 113202

to study their collective motion, several theoretical models have been proposed and explored [7–10]. One such approach considered the biological transport phenomena as an example of driven particle diffusive systems that can be analyzed using totally asymmetric simple exclusion processes (TASEPs) [7, 10]. These are widely known stochastic models that have been extensively studied and employed for investigating various transport phenomena in chemistry, physics and biology [3, 10–16]. The original TASEP model was proposed in 1968 to investigate the kinetics of biopolymerization [17]. Since then these models have been used to provide a better understanding of molecular transport processes in various fields [7, 10, 18]. Such particle systems are frequently described in terms of coarse-grained driven lattice gas models wherein the filament is considered as a one-dimensional (1D) lattice. In TASEP models, the motor proteins are viewed as particles that hop on the linear tracks obeying the hard core exclusion principle under some preassigned dynamical rules. The very rich dynamics of motor protein transport have been explored by incorporating associations, dissociations of particles and other features in numerous TASEP models of biological transport phenomena [19–22]. They have been successfully utilized for clarifying many interesting phenomena such as phase separations, boundary-induced phase transitions, shock formations and symmetry breaking [23–27].

Filament-based intracellular transport involves oppositely directed motor proteins such as kinesins and dyneins whose direction of movement is prescribed by the polarity of biofilaments [1, 2, 4]. These proteins move various cellular cargoes in opposite directions. To describe these processes, multi-species-driven diffusion models have been proposed and explored [10]. Several interesting phenomena, including spontaneous symmetry breaking (SSB) when identical particles moving in opposite directions exhibit different dynamic properties, have been reported [10, 14, 15, 23, 28]. The bridge model was the first model to discuss the existence of the broken symmetry under similar dynamical rules for two distinct types of driven particles on the linear track [28]. In recent years, various versions of the SSB phenomena in bidirectional transport have been extensively explored. Owing to the existence of the oppositely moving molecular motors in different states, studies have been carried out to analyze how the collective motion of motor proteins affects the SSB processes [29, 30]. Further, the understanding of symmetry breaking has also been extended to non-Markovian bidirectional transport processes [31]. However, the mechanisms of symmetry-breaking phenomena are still not fully understood [15, 27, 32].

Stimulated by the bidirectional transport of biological molecular motors along protein filaments, such as the motion of kinesins and dyneins along microtubules and myosins-V and myosins-VI along actin filaments [4, 33], in this paper we investigate the effect of local irreversible dissociations on the dynamics of two types of driven particles that move in opposite directions along a single linear track. It is argued that the localized dissociation sites divide the originally inhomogeneous system into two homogeneous sub-lattices for which theoretical results are known. A new theoretical framework based on mean-field approximations is developed and it is applied for investigating the stationary dynamics, symmetry-breaking phenomena and the dynamic phases in the system. Specifically, we address the following questions: (1) how do the local irreversible dissociations influence the bidirectional transport? (2) For symmetric dissociation rates,

J. Stat. Mech. (2020) 113202

how is the SSB affected by the local dissociations? (3) What changes in the stationary phase diagram take place in systems with local dissociations? To test our theoretical predictions, we also performed extensive Monte Carlo simulations. The proposed theoretical model clarifies some microscopic mechanisms of effective interactions between oppositely moving molecular motors in biological transport phenomena.

2. Model

We consider a finite 1D lattice with N sites, each labeled as $i = 1, 2, \ldots, N$, as shown in figure 1. The sites $i = 1$ and $i = N$ designate the left and right boundaries of the system, respectively, while the sites $i = 2, \ldots, N-1$ correspond to the bulk of the lattice. The progression of two distinct types of particles, labeled as $(+)$ and $(-)$, in opposite directions is allowed on the lattice. The $(+)$ particles move from left to right while the $(-)$ particles move from right to left, as shown in figure 1. The particles obey the hard core exclusion principle that ensures the presence of at most one particle of each kind at a given site. The left boundary, $i = 1$, permits the $(+)$ particle to enter the system with a rate α only if this site is empty. The $(+)$ particles leave the lattice from the site $i = N$ with a rate β. Similarly, the $(-)$ particles are allowed to enter the vacant site $i = N$ with a rate α from the right, and they leave the system from the site $i = 1$ to the left with a rate β. In the bulk, the particles hop to the adjacent empty site in their specified direction with a unit rate. Also, when both types of particles encounter each other on the neighboring sites they swap their positions with a rate q (figure 1). Thus, both types of particles are identical to each other and they can be distinguished only by the direction of their motion.

In addition, we allow both types of particles to irreversibly dissociate from the lattice at the special sites. In the present work, we consider these sites to be far away from the boundaries, and this will ensure that the dissociations do not affect the entrance and exit to the system in the thermodynamic limit ($N \gg 1$). For convenience, it is assumed that these special sites are $k = N/2$ and $k+1$ (figure 1). If the $(+)$ particle is found on the lattice site $i = k$ it can dissociate with a rate δ_+. Similarly, if the $(-)$ particle is found on the lattice site $i = k+1$ it can dissociate with a rate δ_-. The irreversible dissociation of both types of particles and the motion along the lattice are considered equally. This means that the particle at the special site will dissociate with the probability $\delta_\pm/(1+\delta_\pm)$, and the horizontal motion will happen with the probability $1/(1+\delta_\pm)$ if this jump is allowed. For the case when $\delta_+ = \delta_- = 0$, the system reduces to a simple bidirectional transport TASEP model that has been investigated before [23, 28]. The density profiles for particles in the system are characterized by a set of occupancy numbers. Distinctively, τ_i^j, ($i = 1, \ldots, N$ and $j = +, -$) corresponds to the occupancy number of the $(+)$ and $(-)$ particles at the ith site, respectively. Each of them is either 0 (vacant site) or 1 (occupied site).

J. Stat. Mech. (2020) 113202

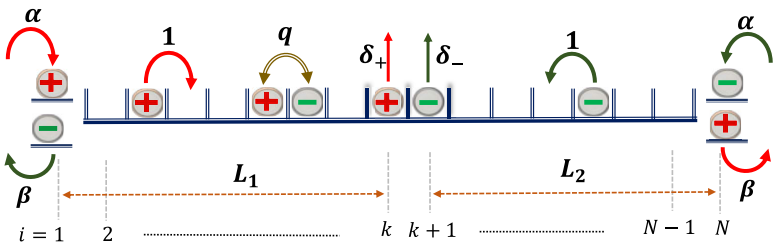

Figure 1. A schematic representation of the bidirectional transport model with local dissociations of the particles at sites far away from the boundaries. Symbols (+) and (−) denote the two types of particles moving in opposite directions: the (+) particles translocate from left to right and the (−) particles translocate from right to left, respectively. The entry and the exit rates for both types of particles are α and β, respectively. In the bulk, the particles hop with the unit rate in their respective directions. The two distinct particles are allowed to swap their position with a rate q when they are found at the neighboring sites. The (+) particle can dissociate from the site $k = N/2$ with the rate δ_+, and the (−) particle can dissociate from the site $k + 1$ with the rate δ_-.

3. Theoretical analysis

Multiple asymmetric exclusion processes with homogeneous bulk dynamics have been successfully analyzed using a variety of theoretical methods [10]. However, the TASEP model for the bidirectional transport with local dissociations considered in this paper has inhomogeneous dynamic rules. This makes it very difficult to apply the known theoretical tools that work for homogeneous systems [10]. At the same time, the inhomogeneity is local, and it divides the lattice into two coupled homogeneous sub-lattices; the left sub-lattice L_1: $i = 1, \ldots, k$ and right sub-lattice L_2: $i = k + 1, \ldots, N$ (figure 1). Now, we can utilize the known results for the homogeneous bidirectional TASEP model to analyze the properties of our model. This approach of mapping the inhomogeneous TASEP model into a coupled homogeneous process has been adopted to study numerous dynamic processes [34–37]. Thus, we view our system as two coupled bidirectional systems with a connection at the special sites k and $k + 1$.

Both sub-lattices can be properly coupled by determining the effective rates for the particles. It is assumed that the (+) particles can exit the left sub-lattice from the site k with the effective exit rate $\beta^+_{\rm eff}$ and they can enter the right sub-lattice at $i = k + 1$ with the effective rate $\alpha^+_{\rm eff}$. Similarly, the (−) particles moving in the opposite direction can leave the right sub-lattice from $i = k + 1$ with the effective rate $\beta^-_{\rm eff}$, and they can enter the left sub-lattice at $i = k$ with the effective rate $\alpha^-_{\rm eff}$. Then using the stationary current arguments, the two sub-lattices can be coupled, and we can explicitly calculate the effective entry and exit rates for both types of particles. After that procedure, employing the results of the homogeneous TASEP model for bidirectional transport we are able investigate the dynamic properties of the two sub-lattices separately.

J. Stat. Mech. (2020) 113202

3.1. Mean-field approximation for homogeneous bidirectional TASEP model

The temporal evolution of the occupancy numbers for (+) and (−) particles can be written as

$$\frac{\mathrm{d}\langle\tau_i^+\rangle}{\mathrm{d}t} = J^+_{i-1,i} - J^+_{i,i+1}, \qquad \frac{\mathrm{d}\langle\tau_i^-\rangle}{\mathrm{d}t} = J^-_{i+1,i} - J^-_{i,i-1}, \tag{1}$$

where $\langle\ldots\rangle$ represents the statistical average over all possible particle configurations. The terms $J^+_{i,i+1}$ and $J^-_{i+1,i}$ denote the currents induced in the bulk of the lattice due to the (+) and (−) particles, respectively, and they are given by

$$J^+_{i,i+1} = \langle\tau_i^+(1-\tau^+_{i+1}-\tau^-_{i+1})\rangle + q\langle\tau_i^+\tau^-_{i+1}\rangle, \tag{2}$$

$$J^-_{i+1,i} = \langle\tau^-_{i+1}(1-\tau_i^+-\tau_i^-)\rangle + q\langle\tau^-_{i+1}\tau_i^+\rangle. \tag{3}$$

At the same time, at the boundaries for the currents we have

$$J^+_{\mathrm{entr}} = \alpha\langle(1-\tau_1^+-\tau_1^-)\rangle, \qquad J^+_{\mathrm{exit}} = \beta\langle\tau_N^+\rangle, \tag{4}$$

$$J^-_{\mathrm{entr}} = \alpha\langle(1-\tau_N^+-\tau_N^-)\rangle, \qquad J^-_{\mathrm{exit}} = \beta\langle\tau_1^-\rangle. \tag{5}$$

As the simplest approach, we assume that the occupancy of the lattice sites is independent of the occupancy status of the neighboring sites,

$$\langle\tau_i^+\tau^+_{i+1}\rangle \approx \langle\tau_i^+\rangle\langle\tau^+_{i+1}\rangle, \qquad \langle\tau_i^-\tau^-_{i+1}\rangle \approx \langle\tau_i^-\rangle\langle\tau^-_{i+1}\rangle, \tag{6}$$

where the average occupation numbers are denoted as,

$$\langle\tau_i^+\rangle = \rho_i^+ \qquad \langle\tau_i^-\rangle = \rho_i^-. \tag{7}$$

This approximation neglects the nearest-neighbor correlations, and it is known as a mean-field approximation. It has been widely utilized in investigations of various TASEP systems [10].

In the stationary state, the particle fluxes become constant and we can label them as J^+ and J^-, respectively. For the case when two different particles swap with the unit rate $q = 1$, the above expressions of current in the bulk ($1 < i < N$) given by equations (2) and (3) reduce to,

$$J^+ = \rho_i^+(1-\rho_i^+), \qquad J^- = \rho_i^-(1-\rho_i^-). \tag{8}$$

Meanwhile, for the boundaries we have

$$J^+ = \alpha(1-\rho_1^+-\rho_1^-), \qquad J^+ = \beta\rho_N^+, \tag{9}$$

$$J^- = \alpha(1-\rho_N^+-\rho_N^-), \qquad J^- = \beta\rho_1^-. \tag{10}$$

When $q = 1$ the particles of different types are effectively interacting with each other only at the boundaries by blocking the entrance/exit sites to particles of other type, and in the bulk the system can be viewed as two independent single-species TASEP models. Since we are interested in understanding the general quantitative features associated

J. Stat. Mech. (2020) 113202

with the presence of local dissociations in the bidirectional transport of driven particles, in this work we focus only on this simplest scenario. In this case, the modified entry rates for the (+) and (−) particles, α^+ at $i = 1$ and α^- at $i = N$, respectively, are explained in [23, 28],

$$\alpha^+ = \frac{J^+}{\frac{J^+}{\alpha} + \frac{J^-}{\beta}}, \qquad \alpha^- = \frac{J^-}{\frac{J^-}{\alpha} + \frac{J^+}{\beta}}. \tag{11}$$

3.2. Coupling of two sub-lattices

In the left sub-lattice L_1, the (+) particles enter with the rate α^+ at $i = 1$ and leave from the site $i = k$ with the rate $\beta^+_{\rm eff}$ whereas the (−) particles enter at the site $i = k$ with the rate $\alpha^-_{\rm eff}$ and escape the lattice from the site $i = 1$ with the rate β. In the right sub-lattice L_2, the (+) particles enter with the rate $\alpha^+_{\rm eff}$ at the site $i = k + 1$ and exit the lattice from $i = N$ with the rate β whereas the (−) particles enter at the site $i = N$ with the rate α^- and move out of the lattice from the site $i = k + 1$ with the rate $\beta^-_{\rm eff}$. We denote the bulk current induced due to the (+) and (−) particles as $J^+_{{\rm bulk},L_j}$ and $J^-_{{\rm bulk},L_j}$, respectively, where $j = 1$ is the left sub-lattice and $j = 2$ the right sub-lattice. Consequently, the modified entry rates in equation (11) are rewritten as,

$$\alpha^+ = \frac{J^+_{{\rm bulk},L_1}}{\frac{J^+_{{\rm bulk},L_1}}{\alpha} + \frac{J^-_{{\rm bulk},L_1}}{\beta}}, \tag{12}$$

$$\alpha^- = \frac{J^-_{{\rm bulk},L_2}}{\frac{J^+_{{\rm bulk},L_2}}{\alpha} + \frac{J^-_{{\rm bulk},L_2}}{\beta}}. \tag{13}$$

Now, the stationarity of the particle flux for the (+) particles requires that the exit current from the left sub-lattice ($J^+_{{\rm exit},L_1}$) at site $i = k$ is equal to the sum of the current due to dissociation of the particle from the kth site and the jump of the particle from site k to $k + 1$, written as,

$$J^+_{{\rm exit},L_1} = J^+_{\rm off} + J^+_{\rm pass}, \tag{14}$$

where

$$J^+_{{\rm exit},L_1} = \beta^+_{\rm eff}\rho^+_k, \qquad J^+_{\rm off} = \delta_+\rho^+_k, \qquad J^+_{\rm pass} = \rho^+_k(1 - \rho^+_{k+1}). \tag{15}$$

Then equation (14) implies that

$$\beta^+_{\rm eff} = \delta_+ + 1 - \rho^+_{k+1}. \tag{16}$$

Also, the current entering into the right sub-lattice L_2 ($J^+_{{\rm entr},L_2}$) at the site $i = k + 1$ is equal to the current that passes from site k to $k + 1$,

$$J^+_{{\rm entr},L_2} = J^+_{\rm pass}, \tag{17}$$

J. Stat. Mech. (2020) 113202

where

$$J^{+}_{\mathrm{entr},L_2} = \alpha^{+}_{\mathrm{eff}}(1-\rho^{+}_{k+1}), \tag{18}$$

leading to

$$\alpha^{+}_{\mathrm{eff}} = \rho^{+}_{k}. \tag{19}$$

Similarly, for the $(-)$ particles progressing in the opposite direction, utilizing the condition of the current stationarity, the current leaving the right sub-lattice L_2 ($J^{-}_{\mathrm{exit},L_2}$) at site $i = k+1$ is equal to the sum of the current induced due to the dissociation of $(-)$ particles from site $i = k+1$ and current passing from site $k+1$ to k, given by,

$$J^{-}_{\mathrm{exit},L_2} = J^{-}_{\mathrm{off}} + J^{-}_{\mathrm{pass}}, \tag{20}$$

where

$$J^{-}_{\mathrm{exit},L_2} = \beta^{-}_{\mathrm{eff}}\rho^{-}_{k+1}, \qquad J^{-}_{\mathrm{pass}} = \rho^{-}_{k+1}(1-\rho^{-}_{k}), \qquad J^{-}_{\mathrm{off}} = \delta_{-}\rho^{-}_{k+1}. \tag{21}$$

Then equation (20) reduces to

$$\beta^{-}_{\mathrm{eff}} = \delta_{-} + 1 - \rho^{-}_{k}. \tag{22}$$

The current that enters into the left sub-lattice L_1 ($J^{-}_{\mathrm{entr},L_1}$) is equal to the current passing from site $k+1$ to k,

$$J^{-}_{\mathrm{entr},L_1} = J^{-}_{\mathrm{pass}}, \tag{23}$$

where

$$J^{-}_{\mathrm{entr},L_1} = \alpha^{-}_{\mathrm{eff}}(1-\rho^{-}_{k}), \tag{24}$$

yielding

$$\alpha^{-}_{\mathrm{eff}} = \rho^{-}_{k+1}. \tag{25}$$

In addition, the current is constant throughout the left and right sub-lattices separately, producing the following relations,

$$\begin{aligned} \alpha^{+}_{\mathrm{eff}}(1-\rho^{+}_{k+1}) &= J^{+}_{\mathrm{bulk},L_2}, \qquad \beta^{+}_{\mathrm{eff}}\rho^{+}_{k} = J^{+}_{\mathrm{bulk},L_1}, \\ \alpha^{-}_{\mathrm{eff}}(1-\rho^{-}_{k}) &= J^{-}_{\mathrm{bulk},L_1}, \qquad \beta^{-}_{\mathrm{eff}}\rho^{-}_{k+1} = J^{-}_{\mathrm{bulk},L_2}. \end{aligned} \tag{26}$$

Substituting ρ^{+}_{k+1}, ρ^{+}_{k}, ρ^{-}_{k} and ρ^{-}_{k+1} from equations (16), (19), (22) and (25) into equation (26), we observe that for the limiting case $\delta_{+} = \delta_{-} = 0$, the above equations reduce to $J^{+}_{\mathrm{bulk},L_1} = J^{+}_{\mathrm{bulk},L_2}$ and $J^{-}_{\mathrm{bulk},L_1} = J^{-}_{\mathrm{bulk},L_2}$, in agreement with the homogeneous bidirectional TASEP model. But for $\delta_{+} \neq 0$ and $\delta_{-} \neq 0$ we obtain the effective entrance/exit rates as follows,

J. Stat. Mech. (2020) 113202

Table 1. Summary of results for a simple homogeneous TASEP model.

	Phase region	ρ_1	ρ_{bulk}	ρ_N	Current (J)
LD	$\alpha < \min\{\beta, 0.5\}$	α	α	$\frac{\alpha(1-\alpha)}{\beta}$	$\alpha(1-\alpha)$
HD	$\beta < \min\{\alpha, 0.5\}$	$1-\frac{\beta(1-\beta)}{\alpha}$	$1-\beta$	$1-\beta$	$\beta(1-\beta)$
MC	$0.5 < \min\{\alpha\beta\}$	$1-\frac{1}{4\alpha}$	0.5	$\frac{1}{4\beta}$	0.25

$$\alpha^{+}_{\text{eff}} = \frac{J^{+}_{\text{bulk},L_1} - J^{+}_{\text{bulk},L_2}}{\delta_{+}}, \tag{27}$$

$$\beta^{+}_{\text{eff}} = \frac{J^{+}_{\text{bulk},L_1}\delta_{+}}{J^{+}_{\text{bulk},L_1} - J^{+}_{\text{bulk},L_2}}, \tag{28}$$

$$\alpha^{-}_{\text{eff}} = \frac{J^{-}_{\text{bulk},L_2} - J^{-}_{\text{bulk},L_1}}{\delta_{-}}, \tag{29}$$

$$\beta^{-}_{\text{eff}} = \frac{J^{-}_{\text{bulk},L_2}\delta_{-}}{J^{-}_{\text{bulk},L_2} - J^{-}_{\text{bulk},L_1}}. \tag{30}$$

These effective rates should help us in quantifying the dynamic phase diagram in the system. Furthermore, we can determine the density profiles for the existing phases.

The simplest version of a homogeneous TASEP model, where a single type of particle enters a 1D lattice with the rate α, hops uni-directionally with the rate 1 and leaves the lattice with the rate β, has been extensively studied [10, 11]. For our theoretical analysis, it is important to recall the main results of this model. There are three distinct stationary phases in this system: low density (LD), high density (HD) and maximal current (MC). For convenience, the conditions of existence, the particle densities and the fluxes for the different phases are summarized in table 1.

3.3. Existence of stationary phases

Let us investigate what stationary phases might exist in the inhomogeneous bidirectional TASEP model. To clarify our discussions, we label the possible phases as $A - B/C - D$, where A and B describe the phases manifested in the left and right sub-lattices, respectively, due to the (+) particles. Similarly, C and D illustrate the phases exhibited by the (−) particles in L_1 and L_2 segments, respectively. In addition, a phase is denoted as a symmetric phase if the bulk density of the (+) particles in L_1 is equal to the bulk density of the (−) particles in L_2 and vice-versa (i.e. $\rho^{+}_{\text{bulk},L_1} = \rho^{-}_{\text{bulk},L_2}$ and $\rho^{-}_{\text{bulk},L_1} = \rho^{+}_{\text{bulk},L_2}$). Otherwise, the phase is designated as an asymmetric phase and labeled in italics.

Since each sub-lattice can be found in one of three phases (MC, LD or HD), the theoretical maximal possible number of stationary phases is $3^4 = 81$. However, the great majority of these phases cannot exist due to various restrictions. For example, because of the irreversible dissociations of the (+) and (−) particles, if the system is in the MC

phase in the entering sub-lattice then it will never reach the MC phase in the exiting sub-lattice. Also, the same sub-lattices cannot exhibit the HD and the MC phases for two different particles simultaneously because the total density at each lattice site cannot exceed 1. It can be shown that all these constraints reduce the number of particles to only six possible dynamic regimes. Let us now discuss explicitly the conditions for the existence of distinct stationary phases.

3.3.1. MC–LD/LD–MC phase. In this phase, the (+) particles exhibit the MC phase in the left sub-lattice L_1 and the LD phase in the right sub-lattice L_2. On the other hand, the (−) particles are in the LD phase in the left sub-lattice L_1 and in the MC phase in the right sub-lattice L_2. The conditions that determine the existence of this phase are the following,

$$0.5 < \min\{\alpha^+, \beta^+_{\rm eff}\}, \qquad \alpha^+_{\rm eff} < \min\{\beta, 0.5\}, \tag{31}$$

$$0.5 < \min\{\alpha^-, \beta^-_{\rm eff}\}, \qquad \alpha^-_{\rm eff} < \min\{\beta, 0.5\}. \tag{32}$$

The currents in the two sub-lattices are given by,

$$J^+_{{\rm bulk},L_1} = 0.25, \qquad J^+_{{\rm bulk},L_2} = \alpha^+_{\rm eff}(1-\alpha^+_{\rm eff}), \tag{33}$$

$$J^-_{{\rm bulk},L_1} = \alpha^-_{\rm eff}(1-\alpha^-_{\rm eff}), \qquad J^-_{{\rm bulk},L_2} = 0.25. \tag{34}$$

We begin by solving equations (33) and (34) using equations (27) and (29), respectively, for the effective entry rates of two distinct particles, yielding

$$\alpha^\pm_{\rm eff} = \frac{1}{2}\left[1+\delta_\pm - \sqrt{\delta_\pm(2+\delta_\pm)}\right]. \tag{35}$$

The effective exit rates are then computed by solving equations (28) and (30),

$$\beta^\pm_{\rm eff} = \frac{1}{4\alpha^\pm_{\rm eff}}. \tag{36}$$

At the boundaries, the modified entry rates are evaluated by substituting the expressions of the current from equations (33) and (34) into equations (12) and (13), producing

$$\alpha^\pm = \frac{\alpha\beta}{\beta + \alpha(1-4\delta_\mp\alpha^\mp_{\rm eff})}. \tag{37}$$

The explicit expressions of the effective entry and exit rates, and the modified entry rates simultaneously satisfying equations (31) and (32) help us to evaluate the region of existence of this phase for a general set of values of the dissociation rates. In addition, the calculated densities in each sub-lattice are summarized in table 2.

One can easily observe that for the symmetric rates $\delta_+ = \delta_-$ from equations (35)–(37) we have $\alpha^+ = \alpha^-$, $\alpha^+_{\rm eff} = \alpha^-_{\rm eff}$ and $\beta^+_{\rm eff} = \beta^-_{\rm eff}$. As a result, the density of the (+) particles in $L_1(L_2)$ is equal to the density of the (−) particles in $L_2(L_1)$ that classifies this dynamic regime as the symmetric phase. However, for the asymmetric dissociation rates $\delta_+ \neq \delta_-$, we have $\alpha^+ \neq \alpha^-$, $\alpha^+_{\rm eff} \neq \alpha^-_{\rm eff}$ and $\beta^+_{\rm eff} \neq \beta^-_{\rm eff}$. Then the densities of the particles in the LD

Table 2. Densities in the MC–LD/LD–MC phase.

	ρ_1	ρ_{bulk,L_1}	ρ_k	ρ_{k+1}	ρ_{bulk,L_2}	ρ_N
(+)	$1-\frac{1}{4\alpha^+}$	0.5	$\frac{1}{4\beta^+_{\text{eff}}}$	α^+_{eff}	α^+_{eff}	$\frac{\alpha^+_{\text{eff}}(1-\alpha^+_{\text{eff}})}{\beta}$
(−)	$\frac{\alpha^-_{\text{eff}}(1-\alpha^-_{\text{eff}})}{\beta}$	α^-_{eff}	α^-_{eff}	$\frac{1}{4\beta^-_{\text{eff}}}$	0.5	$1-\frac{1}{4\alpha^-}$

phase are unequal to each other, making MC–LD/LD–MC in this case the asymmetric phase. Furthermore, for $\delta_+ = \delta_- = 0$, equations (35)–(37) reduce to $\alpha^{\pm}_{\text{eff}} = \frac{1}{2}$, $\beta^{\pm}_{\text{eff}} = \frac{1}{2}$ and $\alpha_{\pm} = \frac{\alpha\beta}{\alpha+\beta}$ that agrees with the existence of the MC/MC phase for the bidirectional homogeneous TASEP model [23, 28].

3.3.2. LD–HD/LD–LD phase. Without any loss of generality, we might consider the (+) particles to be in the LD phase in the L_1 segment and in the HD phase in the L_2 segment. At the same time, the (−) particles are in the LD phase in both sub-lattices L_1 and L_2. The LD–HD/LD–LD phase is specified by the following conditions,

$$\alpha^+ < \min\{\beta^+_{\text{eff}}, 0.5\}, \qquad \beta < \min\{\alpha^+_{\text{eff}}, 0.5\}, \tag{38}$$

$$\alpha^- < \min\{\beta_{\text{eff}}, 0.5\}, \qquad \alpha^-_{\text{eff}} < \min\{\beta, 0.5\}. \tag{39}$$

The bulk currents in both the sub-lattices are given by,

$$J^+_{\text{bulk},L_1} = \alpha^+(1-\alpha^+), \qquad J^+_{\text{bulk},L_2} = \beta(1-\beta), \tag{40}$$

$$J^-_{\text{bulk},L_1} = \alpha^-_{\text{eff}}(1-\alpha^-_{\text{eff}}), \qquad J^-_{\text{bulk},L_2} = \alpha^-(1-\alpha^-). \tag{41}$$

Substituting the current expressions from equations (40) and (41) into (13) gives us the modified entry rate for the (−) particles,

$$\alpha^- = \frac{1+\alpha-\sqrt{(1+\alpha)^2-4\alpha\beta}}{2}. \tag{42}$$

Further, solving equation (29) provides the expression of the effective entry rate α^-_{eff} as,

$$\alpha^-_{\text{eff}} = \frac{1+\delta_- - \sqrt{4\alpha(\alpha^- - \beta)+(1-\delta_-)^2}}{2}. \tag{43}$$

Now, using the current in each sub-lattice from equation (30) leads to the effective exit rate of the (−) particles from L_2,

$$\beta^-_{\text{eff}} = \frac{\alpha(2\beta-\alpha^-)}{2\alpha^-_{\text{eff}}}. \tag{44}$$

Next, the modified entry rate α^+ is computed from equation (12),

$$\alpha^+ = \frac{1}{2}\left(1+\alpha-\sqrt{\frac{4\alpha J^-_{\text{bulk},L_1}}{\beta}+(1-\alpha)^2}\right) \tag{45}$$

J. Stat. Mech. (2020) 113202

Table 3. Densities in the LD–HD/LD–LD phase.

	ρ_1	ρ_{bulk,L_1}	ρ_k	ρ_{k+1}	ρ_{bulk,L_2}	ρ_N
$(+)$	α^+	α^+	$\frac{\alpha^+(1-\alpha^+)}{\beta^+_{\text{eff}}}$	$1-\frac{\beta(1-\beta)}{\alpha^+_{\text{eff}}}$	$1-\beta$	$1-\beta$
$(-)$	$\frac{\alpha^-_{\text{eff}}(1-\alpha^-_{\text{eff}})}{\beta}$	α^-_{eff}	α^-_{eff}	$\frac{\alpha^-(1-\alpha^-)}{\beta^-_{\text{eff}}}$	α^-	α^-

which is used in equations (27) and (28) to obtain α^+_{eff} and β^+_{eff}. These expressions are then utilized to determine the parameter range of this phase that satisfies equations (38) and (39) for varying values of the dissociation rates. The corresponding densities in the two sub-lattices are summarized in table 3.

Now, one can clearly observe that, whether the dissociation rates are symmetric or asymmetric, the sub-lattice L_2 being in the HD phase for the $(+)$ particles displays $\rho^+_{\text{bulk},L_2} > 0.5$ and the sub-lattice L_1 being in the LD phase for the $(-)$ particles shows $\rho^-_{\text{bulk},L_1} < 0.5$. Hence, the densities in the two sub-lattices always remain unequal to each other, and this stationary regime is always the asymmetric phase.

3.3.3. HD–HD/LD–LD phase. Using a similar approach, we assume that the $(+)$ particles are in the HD phase in both the sub-lattices, while the $(-)$ particles are in the LD phase in both sub-lattices. This phase exists when,

$$\beta^+_{\text{eff}} < \min\{\alpha^+, 0.5\}, \qquad \beta < \min\{\alpha^+_{\text{eff}}, 0.5\}, \tag{46}$$

$$\alpha^- < \min\{\beta^-_{\text{eff}}, 0.5\}, \qquad \alpha^-_{\text{eff}} < \min\{\beta, 0.5\}. \tag{47}$$

For this phase, the particle fluxes in the sub-lattices are given by,

$$J^+_{\text{bulk},L_1} = \beta^+_{\text{eff}}(1-\beta^+_{\text{eff}}), \qquad J^+_{\text{bulk},L_2} = \beta(1-\beta), \tag{48}$$

$$J^-_{\text{bulk},L_1} = \alpha^-_{\text{eff}}(1-\alpha^-_{\text{eff}}), \qquad J^-_{\text{bulk},L_2} = \alpha^-(1-\alpha^-). \tag{49}$$

Using equation (28), we first evaluate the effective exit rate for the $(+)$ particles from the left sub-lattice L_1,

$$\beta^+_{\text{eff}} = \frac{1+\delta_+ - \sqrt{(1-2\beta)^2 + \delta_+(\delta_+ - 2)}}{2}. \tag{50}$$

Since $\beta^+_{\text{eff}} < 0.5$, the above equation leads to the following inequality,

$$\beta < \frac{1-\sqrt{2\delta_+}}{2}, \tag{51}$$

which implies that this phase exists only when $\delta_+ < 0.5$. The modified and the effective entry rates for the $(+)$ particles are obtained by solving equations (12) and (27), respectively, yielding

$$\alpha^+_{\text{eff}} = \frac{1-\delta_+ + \sqrt{(\delta_+ - 1)^2 - 4J^+_{\text{bulk},L_2}}}{2}, \qquad \alpha^+ = \frac{\alpha A}{2\alpha J^-_{\text{bulk},L_1} + A} \tag{52}$$

J. Stat. Mech. (2020) 113202

Table 4. Densities in the HD–HD/LD–LD phase.

	ρ_1	ρ_{bulk,L_1}	ρ_k	ρ_{k+1}	ρ_{bulk,L_2}	ρ_N
(+)	$1-\frac{\beta^+_{\text{eff}}(1-\beta^+_{\text{eff}})}{\alpha^+}$	$1-\beta^+_{\text{eff}}$	$1-\beta^+_{\text{eff}}$	$1-\frac{\beta(1-\beta)}{\alpha^+_{\text{eff}}}$	$1-\beta$	$1-\beta$
(−)	$\frac{\alpha^-_{\text{eff}}(1-\alpha^-_{\text{eff}})}{\beta}$	α^-_{eff}	α^-_{eff}	$\frac{\alpha^-(1-\alpha^-)}{\beta^-_{\text{eff}}}$	α^-	α^-

where

$$A = \beta\left[2J^+_{\text{bulk},L_2} + \delta_+(2\beta^+_{\text{eff}} - 1)\right]. \tag{53}$$

Now, since the (−) particles are in the LD phase in both sub-lattices, the expressions for the corresponding effective and modified rates are given by equations (42)–(44). Combining all the obtained expressions for entry and exit for two distinct particles, depending on the conditions presented in equations (46) and (47) one can specify the conditions for the existence of this dynamic regime. For this phase, the densities of both types of particles are given in table 4. Since the (+) particles exhibit the HD phase in both sub-lattices, the density is greater than 0.5, whereas (−) particles are in the LD phase for which L_1 and L_2 exhibit a density less than 0.5. As a consequence, whether the dissociation rate is symmetric or asymmetric, this phase is always an asymmetric phase. For the limiting case $\delta_+ = \delta_- = 0$, the conditions for this phase reduce to HD/LD phase with uniform density as observed in bidirectional homogeneous systems [23, 28].

3.3.4. MC–LD/LD–LD phase. For this phase, let us assume for convenience that the (+) particles are in the MC and in the LD phases in sub-lattices L_1 and L_2, respectively. At the same time, both sub-lattices must have the LD phase for the (−) particles. The conditions for the existence of this phase satisfy

$$0.5 < \min\{\alpha^+, \beta^+_{\text{eff}}\}, \qquad \alpha^+_{\text{eff}} < \min\{\beta, 0.5\}, \tag{54}$$

$$\alpha^- < \min\{\beta^-_{\text{eff}}, 0.5\}, \qquad \alpha^-_{\text{eff}} < \min\{\beta, 0.5\}. \tag{55}$$

The bulk currents in the sub-lattices are expressed as,

$$J^+_{\text{bulk},L_1} = 0.25, \qquad J^+_{\text{bulk},L_2} = \alpha^+_{\text{eff}}(1-\alpha^+_{\text{eff}}), \tag{56}$$

$$J^-_{\text{bulk},L_1} = \alpha^-_{\text{eff}}(1-\alpha^-_{\text{eff}}), \qquad J^-_{\text{bulk},L_2} = \alpha^-(1-\alpha^-). \tag{57}$$

The effective and modified entry and exit rates for the (+) particles have already been computed in equations (35)–(37). The expression of α^+_{eff} can now be utilized to evaluate the modified entry rate for the (−) particles (α^-) from equation (13),

$$\alpha^- = \frac{1}{2}\left(1+\alpha-\sqrt{\frac{4\alpha J^+_{\text{bulk},L_2}}{\beta}+(1-\alpha)^2}\right) \tag{58}$$

J. Stat. Mech. (2020) 113202

Table 5. Densities in the MC–LD/LD–LD phase.

	ρ_1	ρ_{bulk,L_1}	ρ_k	ρ_{k+1}	ρ_{bulk,L_2}	ρ_N
(+)	$1-\frac{1}{4\alpha^+}$	0.5	$\frac{1}{4\beta^+_{\text{eff}}}$	α^+_{eff}	α^+_{eff}	$\frac{\alpha^+_{\text{eff}}(1-\alpha^+_{\text{eff}})}{\beta}$
(−)	$\frac{\alpha^-_{\text{eff}}(1-\alpha^-_{\text{eff}})}{\beta}$	α^-_{eff}	α^-_{eff}	$\frac{\alpha^-(1-\alpha^-)}{\beta^-_{\text{eff}}}$	α^-	α^-

Using equation (29), the effective entry rate of the (−) particles into the L_2 segment is given by,

$$\alpha^-_{\text{eff}} = \frac{1+\delta_- - \sqrt{(1+\delta_-)^2 - 4J^-_{\text{bulk},L_2}}}{2} \tag{59}$$

Further, utilizing the current induced in L_1 and L_2 due to the (−) particles, equation (30) provides the effective exit rate β^-_{eff}. These explicit relations determine the region satisfying equations (54) and (55) that describes the MC–LD/LD–LD phase in the stationary regime. In each of the sub-lattices, the densities of two types of particles are summarized in table 5.

One can see that in the left sub-lattice L_1, the bulk density of the (+) particles is 0.5 while in the right sub-lattice L_2, the (−) particles exhibit the LD phase where the density is less than 0.5. Hence, there is no pair of dissociation rates δ_+ and δ_- for which $\rho^+_{\text{bulk},L_1} = \rho^-_{\text{bulk},L_2} = 0.5$. This shows that the MC − LD/LD − LD phase is always the asymmetric phase for any chosen values of the dissociation rates.

3.3.5. MC–HD/LD–LD phase. In this phase, we again assume that the (+) particles are in the MC phase in the left sub-lattice and in the HD phase in the right sub-lattice, while the (−) particles are in the LD phase in both sub-lattices. The conditions that determine the existence of the MC–HD/LD–LD phase are

$$0.5 < \min\{\alpha^+, \beta^+_{\text{eff}}\}, \qquad \beta < \min\{\alpha^+_{\text{eff}}, 0.5\}, \tag{60}$$

$$\alpha^- < \min\{\beta^-_{\text{eff}}, 0.5\}, \qquad \alpha^-_{\text{eff}} < \min\{\beta, 0.5\}. \tag{61}$$

The particle fluxes are given by,

$$J^+_{\text{bulk},L_1} = 0.25, \qquad J^+_{\text{bulk},L_2} = \beta(1-\beta), \tag{62}$$

$$J^-_{\text{bulk},L_1} = \alpha^-_{\text{eff}}(1-\alpha^-_{\text{eff}}), \qquad J^-_{\text{bulk},L_2} = \alpha^-(1-\alpha^-). \tag{63}$$

The effective and modified rates for the (−) particles have already been evaluated above in equations (42)–(44). The effective entry rate of the (+) particles into the right sub-lattice is obtained by solving equation (27) that yields,

$$\alpha^+_{\text{eff}} = \frac{(2\beta-1)^2}{4\delta_+}. \tag{64}$$

J. Stat. Mech. (2020) 113202

Table 6. Densities in the MC–HD/LD–LD phase.

	ρ_1	ρ_{bulk,L_1}	ρ_k	ρ_{k+1}	ρ_{bulk,L_2}	ρ_N
(+)	$1-\frac{1}{4\alpha^+}$	0.5	$\frac{1}{4\beta^+_{\text{eff}}}$	α^+_{eff}	$1-\beta$	$1-\beta$
(−)	$\frac{\alpha^-_{\text{eff}}(1-\alpha^-_{\text{eff}})}{\beta}$	α^-_{eff}	α^-_{eff}	$\frac{\alpha^-(1-\alpha^-)}{\beta^-_{\text{eff}}}$	α^-	α^-

Utilizing the bulk current expressions from equations (62) and (63) in equation (28) yields

$$\beta^+_{\text{eff}} = \frac{\delta_+}{1-4\beta(1-\beta)}. \tag{65}$$

The modified entry rate of the (+) particles entering the left sub-lattice is evaluated from equation (12). The parameter range for which this phase exists is determined by the conditions given in equations (60) and (61). The particle densities in the L_1 and L_2 segments are summarized in table 6.

Furthermore, the (+) particles are in the MC phase in the sub-lattice L_1, and the corresponding bulk density for these particles is 0.5. At the same time, the bulk density of the (−) particles in L_2 is less than 0.5. Therefore, for no values of δ_+ and δ_- we can have $\rho^+_{\text{bulk},L_1} = \rho^-_{\text{bulk},L_2}$. This observation suggests that the MC–HD/LD–LD phase is also always the asymmetric phase.

3.3.6. LD–LD/LD–LD phase. In this phase, the two types of particles are in the LD phase in both sub-lattices L_1 and L_2. The conditions that specify the existence of this phase are,

$$\alpha^+ < \min\{\beta^+_{\text{eff}}, 0.5\}, \qquad \alpha^+_{\text{eff}} < \min\{\beta, 0.5\}, \tag{66}$$

$$\alpha^- < \min\{\beta^-_{\text{eff}}, 0.5\}, \qquad \alpha^-_{\text{eff}} < \min\{\beta, 0.5\}. \tag{67}$$

The particle currents in the system are given by,

$$J^+_{\text{bulk},L_1} = \alpha^+(1-\alpha^+), \qquad J^+_{\text{bulk},L_2} = \alpha^+_{\text{eff}}(1-\alpha^+_{\text{eff}}), \tag{68}$$

$$J^-_{\text{bulk},L_1} = \alpha^-_{\text{eff}}(1-\alpha^-_{\text{eff}}), \qquad J^-_{\text{bulk},L_2} = \alpha^-(1-\alpha^-). \tag{69}$$

We obtain the modified entry rates by solving equations (12) and (13), producing

$$\alpha^+ = \frac{1}{2}\left(1+\alpha+\sqrt{\frac{4\alpha J^-_{\text{bulk},L_1}}{\beta}+(1-\alpha)^2}\right), \tag{70}$$

$$\alpha^- = \frac{1}{2}\left(1+\alpha+\sqrt{\frac{4\alpha J^+_{\text{bulk},L_2}}{\beta}+(1-\alpha)^2}\right). \tag{71}$$

Table 7. Density in LD–LD/LD–LD phase.

	ρ_1	ρ_{bulk,L_1}	ρ_k	ρ_{k+1}	ρ_{bulk,L_2}	ρ_N
(+)	α^+	α^+	$\frac{\alpha^+(1-\alpha^+)}{\beta^+_{\text{eff}}}$	α^+_{eff}	α^+_{eff}	$\frac{\alpha^+_{\text{eff}}(1-\alpha^+_{\text{eff}})}{\beta}$
(−)	$\frac{\alpha^-_{\text{eff}}(1-\alpha^-_{\text{eff}})}{\beta}$	α^-_{eff}	α^-_{eff}	$\frac{\alpha^-(1-\alpha^-)}{\beta^-_{\text{eff}}}$	α^-	α^-

Further, solving equations (27)–(30) provides the following expressions for the effective entry and exit rates,

$$\alpha^+_{\text{eff}} = \frac{1+\delta_+ - \sqrt{(\delta_+ + 1)^2 - 4J^+_{\text{bulk},L_1}}}{2}, \qquad \beta^+_{\text{eff}} = \frac{J^+_{\text{bulk},L_1}}{\alpha^+_{\text{eff}}}, \tag{72}$$

$$\alpha^-_{\text{eff}} = \frac{1+\delta_- - \sqrt{(\delta_- + 1)^2 - 4J^-_{\text{bulk},L_2}}}{2}, \qquad \beta^-_{\text{eff}} = \frac{J^-_{\text{bulk},L_2}}{\alpha^-_{\text{eff}}}. \tag{73}$$

As before, we summarize the particle densities in both sub-lattices in table 7.

Since both types of particles are in the LD phase in the left and right sub-lattices, this phase can be symmetric. But at the same time, we might have $\rho^+_{\text{bulk},L_1} \neq \rho^-_{\text{bulk},L_2}$ and $\rho^-_{\text{bulk},L_1} \neq \rho^+_{\text{bulk},L_2}$, and this suggests that this phase might also be asymmetric. Thus, we predict that depending on the values and symmetry of the dissociation rates, the LD–LD/LD–LD phase might be symmetric or asymmetric.

4. Results and discussions

Our theoretical approach involves several approximations, and in order to test its validity we performed extensive Monte Carlo simulations for the bidirectional transport of driven particles with local dissociations. The computer simulations are carried out by considering lattices with a size $N = 1000$ for 2×10^9 time steps and neglecting the first 5% of the time steps to ensure that the system reaches the steady state. We analyze the system dynamics for two different scenarios: when the dissociation rates are symmetric, $\delta_+ = \delta_- = \delta$, and when the dissociation rates are asymmetric, $\delta_+ \neq \delta_-$.

4.1. Case 1: symmetric dissociation rates ($\delta_+ = \delta_- = \delta$) and SSB

To explore the effect of dissociation rates on the properties of the system, we investigate the possible stationary phases by varying the entrance and exit rates α and β. In the special case $\delta = 0$, our model reduces to a well-studied homogeneous bidirectional TASEP model [23, 28]. To better understand the dynamic properties of our system with dissociations, we begin our discussions by recalling the important features of the model without dissociations. The phase diagram for this limiting case is presented in

J. Stat. Mech. (2020) 113202

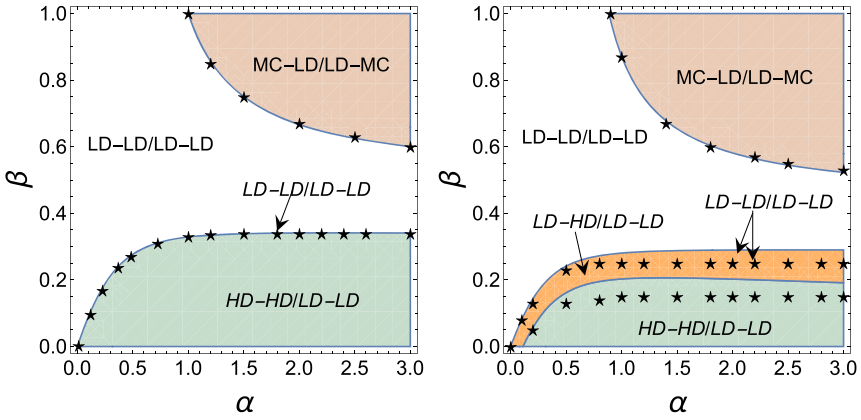

(a) $\delta = 0$

(b) $\delta = 0.1$

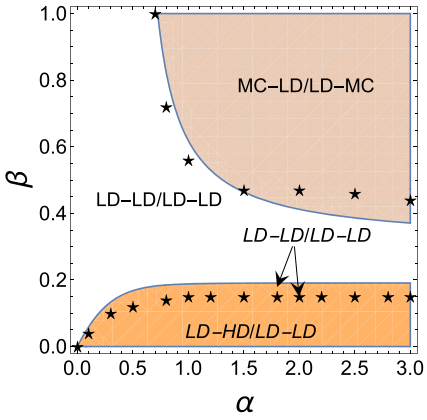

(c) $\delta = 0.5$

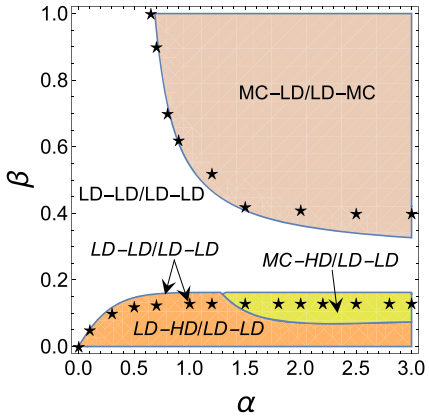

(d) $\delta = 0.7$

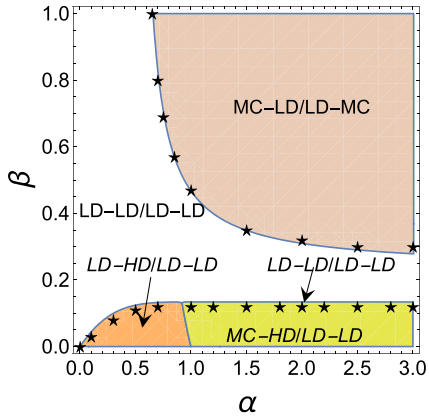

(e) $\delta = 1$

Figure 2. Stationary phase diagrams for (a) $\delta = 0$, (b) $\delta = 0.1$, (c) $\delta = 0.5$, (d) $\delta = 0.7$, (e) $\delta = 1$. Solid lines are the phase boundaries obtained theoretically. Symbols represent the Monte Carlo simulations results. Note that the asymmetric LD–LD/LD–LD phase is at the border line between the symmetric LD–LD/LD–LD and other asymmetric phases. Asymmetric phases are labeled in italics.

J. Stat. Mech. (2020) 113202

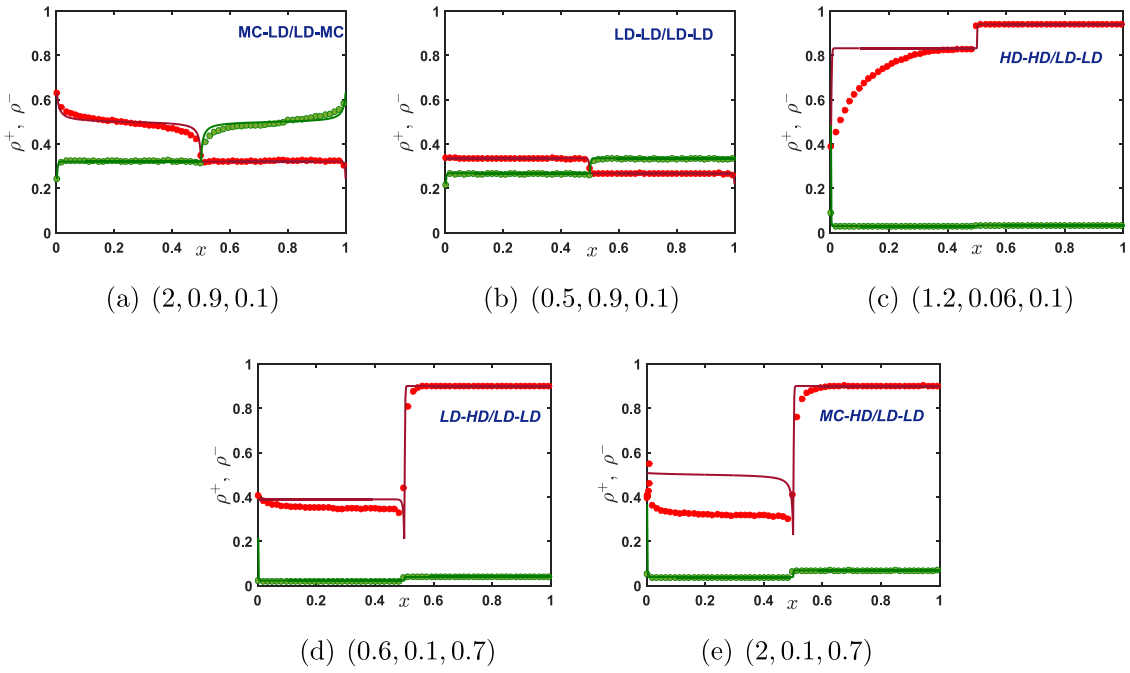

(a) $(2, 0.9, 0.1)$ (b) $(0.5, 0.9, 0.1)$ (c) $(1.2, 0.06, 0.1)$

(d) $(0.6, 0.1, 0.7)$ (e) $(2, 0.1, 0.7)$

Figure 3. Average density profiles for different stationary phases with symmetric dissociation rates $\delta_+ = \delta_- = \delta$. (a), (b) The symmetric density profiles, whereas (c)–(e) are the asymmetric profiles. The parameter set (α, β, δ) is given in the sub-caption of each density profile. Red and green filled markers are the simulated results for $(+)$ and $(-)$ particles, respectively. Corresponding red and green solid lines are theoretical results that are in good agreement with Monte Carlo simulations.

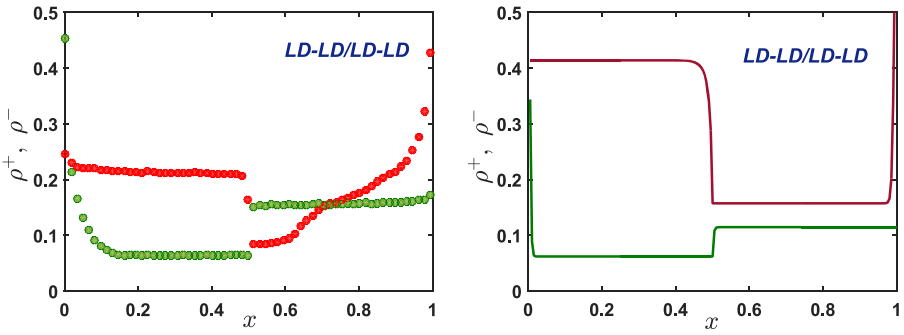

(a) $(0.5, 0.129, 0.7)$ (b) $(0.5, 0.169, 0.7)$

Figure 4. Average density profiles for asymmetric LD–LD/LD–LD phase with symmetric dissociation rates which is found to be restricted to a line. Since the theoretical phase boundaries are not in exact agreement with simulations, we present it as a density profile for two different sets of parameters with simulations and theory in (a) and (b) respectively for (α, β, δ) stated in sub-captions.

J. Stat. Mech. (2020) 113202

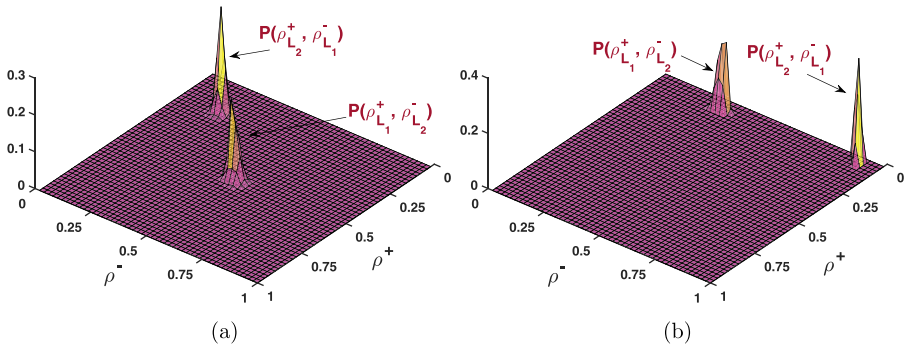

Figure 5. Particle density histograms $P(\rho^{+}_{L_1}, \rho^{-}_{L_2})$ and $P(\rho^{-}_{L_1}, \rho^{+}_{L_2})$ for the symmetric dissociation rate $\delta = 0.5$: (a) symmetric phase MC–LD/LD–MC with $\alpha = 2.5$, $\beta = 0.9$ where we can clearly observe $\rho^{+}_{L_1} = \rho^{-}_{L_2} = 0.5$ and $\rho^{-}_{L_1} = \rho^{+}_{L_2} = 0.2 < 0.5$; and (b) asymmetric phase LD–HD/LD–LD with $\alpha = 2.5$, $\beta = 0.1$ where $\rho^{+}_{L_1} = 0.08$, $\rho^{-}_{L_2} = 0.32$, $\rho^{+}_{L_2} = 0.06$ and $\rho^{-}_{L_1} = 0.9$ that satisfies $\rho^{+}_{L_1} < \rho^{-}_{L_2} < 0.5$, $\rho^{+}_{L_2} < 0.5$ and $\rho^{-}_{L_1} > 0.5$.

figure 2(a). It was found that there are two symmetric phases: MC–LD/LD–MC and LD–LD/LD–LD. Despite the symmetry of transition rates for the (+) and (−) particles, the system also exhibits two asymmetric phases, LD–LD/LD–LD and HD–HD/LD–LD. Calculations also show that in the thermodynamic limit the region of existence for the LD–LD/LD–LD phase is restricted to a line corresponding to the border between the symmetric LD–LD/LD–LD and asymmetric HD–HD/LD–LD phases. Since no bulk-induced dynamics are involved in the homogeneous system, the density of both particles remains uniform throughout the lattice.

Introducing the dissociation rate δ breaks the translational symmetry of the system and it changes the stationary phase diagram. We observed that as soon as δ becomes non-zero, the number of phases increases from four to five in comparison to that obtained for $\delta = 0$. A new asymmetric phase LD–HD/LD–LD appears as shown for $\delta = 0.1$ in figure 2(b). Further increase in the dissociation rate eliminates the asymmetric phase HD–HD/LD–LD for $\delta \geqslant 0.5$. This is because the rate of leaving the sub-lattice L_1 becomes too large and it violates the condition for the existence of this phase given in equation (51) ($\beta < \frac{1-\sqrt{2\delta}}{2}$). Four stationary phases (two symmetric and two asymmetric) are observed for $\delta = 0.5$ as presented in figure 2(c). In addition, due to the significant increase in the effective exit rate β^{+}_{eff}, the symmetric MC–LD/LD–MC phase expands. This also leads to the appearance of a new asymmetric MC–HD/LD–LD phase in the stationary diagram, which grows with the increase in the dissociation rate; see figures 2(d) and (e).

The density profiles for systems with symmetric dissociation rates are presented in figure 3. One can clearly distinguish the symmetric phases (figures 3(a) and (b)) where the density profiles are symmetric with respect to the location of the dissociation sites ($x = 0.5$) from the asymmetric phases (figures 3(c)–(e) and 4) where such symmetry is broken. We also notice that our mean-field theoretical approach is excellent in describing the symmetric phase, while it has only limited success for the asymmetric phases. The

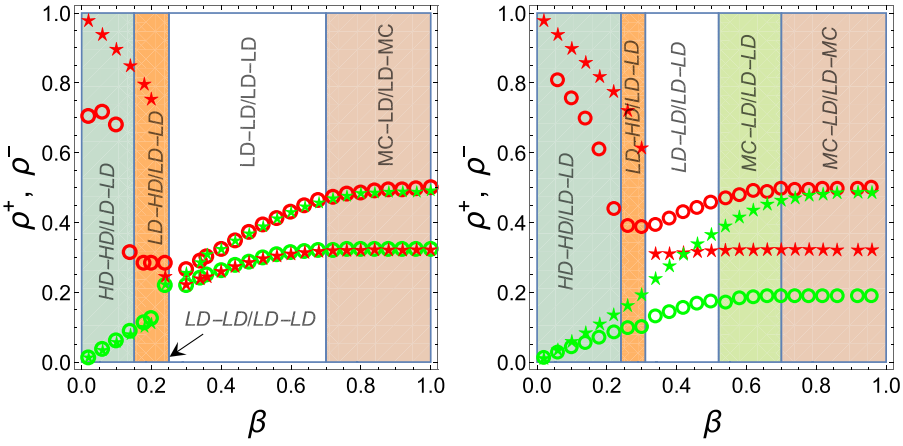

Figure 6. Bulk densities at the peaks of distributions calculated via Monte Carlo simulations for increasing rate β with the fixed rate $\alpha = 1.5$. (a) Symmetric dissociation rate $\delta = 0.1$. (b) Asymmetric dissociation rates $\delta_+ = 0.5$ and $\delta_- = 0.1$. The two types of particles (+) and (−) are represented in red and green color, respectively. Open circles and stars denote the density of particles on sub-lattice L_1 and L_2, respectively.

computer simulation results for densities in some sub-lattices agree only qualitatively with theoretical predictions. In addition, the location of phase boundaries is not in exact agreement with Monte Carlo simulations.

One of the most striking features of the bidirectional transport of driven particles is the observation of the SSB. To investigate this phenomenon in a system with local dissociations via Monte Carlo simulations, we probe particle density histograms $P(\rho^+_{L_1}, \rho^-_{L_2})$ and $P(\rho^-_{L_1}, \rho^+_{L_2})$ where $\rho^+_{L_i}$ and $\rho^-_{L_i}$ are the instantaneous densities of the (+) and (−) particles, respectively, on the sub-lattice L_i $(i = 1, 2)$. Here, we chose such pairs because the occurrence of the symmetric and asymmetric phase depends on the particle density of the (+) particles in L_1 and the (−) particles in L_2, and on the (+) particles in L_2 and the (−) particles in L_1. A phase is labeled as a symmetric phase for the case when the peaks in density distribution satisfy $\rho^+_{L_1} = \rho^-_{L_2}$ and $\rho^-_{L_1} = \rho^+_{L_2}$, otherwise the phase is labeled as an asymmetric phase. For the symmetric dissociation rate $\delta = 0.5$, typical density histograms for the symmetric MC–LD/LD–MC and the asymmetric LD–HD/LD–LD phases are presented in figure 5. One can see in figure 5(b) that the peaks in the distributions are achieved for $\rho^+_{L_1} = \rho^-_{L_2} = 0.5$ and $\rho^+_{L_2} = \rho^-_{L_1} < 0.5$ that correspond to the symmetric MC–LD/LD–MC phase. Figure 5(b) demonstrates that the peaks occur for $\rho^+_{L_1} < \rho^-_{L_2} < 0.5$ and for $\rho^+_{L_2} < 0.5$ and $\rho^-_{L_1} > 0.5$, which corresponds to the asymmetric LD–HD/LD–LD phase. One can also observe the symmetry breaking by monitoring the changes in the densities during the phase transitions as illustrated in figure 6 for a fixed value of $\alpha = 1.5$. Figure 6(a) presents the case of the symmetric dissociation rates where the SSB phenomenon might be observed in the system. We found that for smaller values of the rate β, the density of (+) particles in $L_1(L_2)$ [represented by red open circles (stars)] is not equal to the density of (−) particles in $L_2(L_1)$ [represented

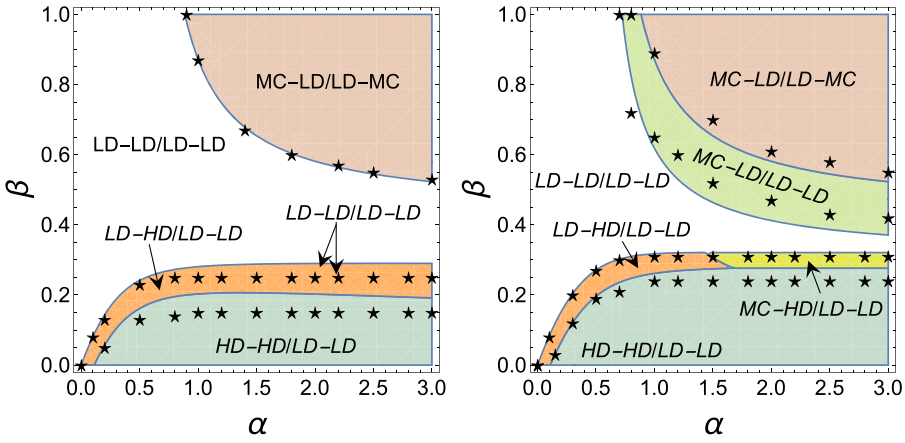

(a) $\delta_+ = 0.1$, $\delta_- = 0.1$ (b) $\delta_+ = 0.5$, $\delta_- = 0.1$

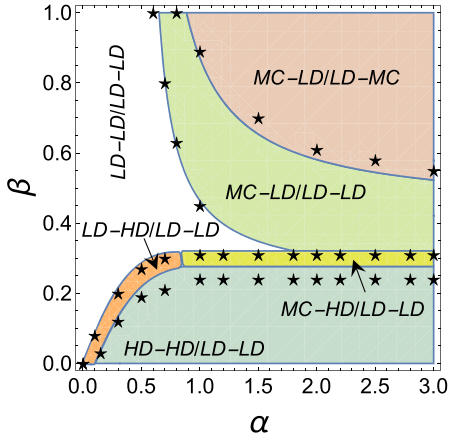

(c) $\delta_+ = 1$, $\delta_- = 0.1$

Figure 7. Stationary phase diagrams for increasing the dissociation rate δ_+ with the fixed dissociation rate $\delta_- = 0.1$. Solid lines are theoretical phase boundaries, while symbols represent the results from simulations.

by green stars (open circles)], and this corresponds to the asymmetric phases, whereas beyond a critical value of the rate β these densities are always equal to each other, which corresponds to the symmetric phases. Based on similar arguments, for the asymmetric dissociation rates, figure 6(b) illustrates the possibility of having only the asymmetric phase for all values of β. These results indicate that the SSB phenomena occur even in bidirectional transport with local dissociations. The dissociations only affect the nature of the emerging asymmetric phases.

4.2. Case 2: asymmetric dissociation rates ($\delta_+ \neq \delta_-$)

Now let us investigate the bidirectional transport when the dissociation rates of the two distinct particles are asymmetric $\delta_+ \neq \delta_-$ and the SSB phenomena cannot happen. Due to the different dissociation rates, even if both particles exhibit the same phase

J. Stat. Mech. (2020) 113202

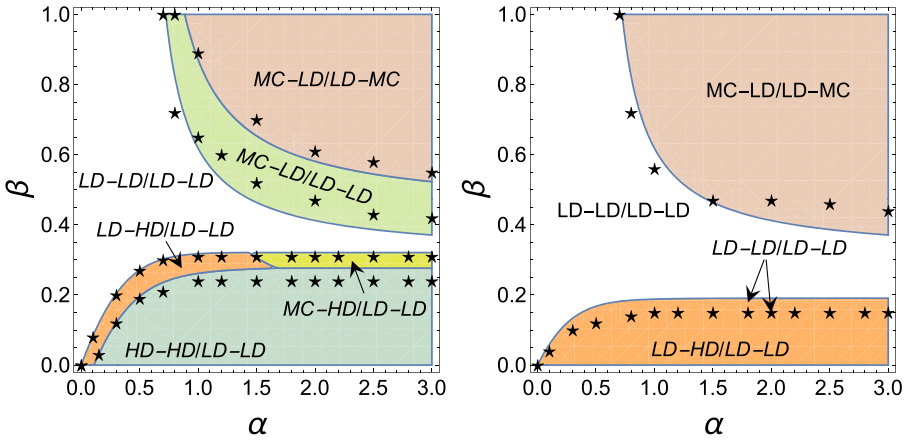

(a) $\delta_+ = 0.1$, $\delta_- = 0.5$

(b) $\delta_+ = 0.5$, $\delta_- = 0.5$

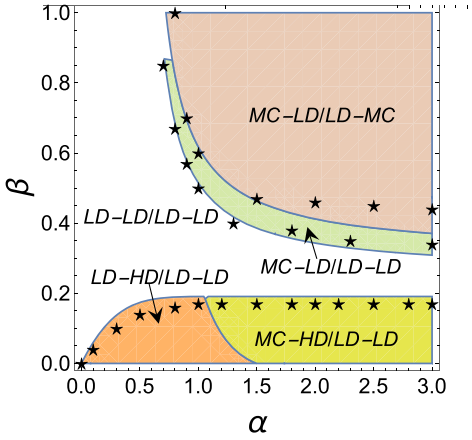

(c) $\delta_+ = 0.8$, $\delta_- = 0.5$

Figure 8. Stationary phase diagrams for increasing the dissociation rate δ_+ with the fixed dissociation rate $\delta_- = 0.5$. Solid lines are theoretical phase boundaries, while symbols represent the results from simulations.

the densities of (+) and (−) particles are not equal in the sub-lattices. Therefore, only asymmetric phases exist in the system.

To explore the effect of asymmetric dissociation rates on the topology of stationary phase diagrams, we investigate our system for three different cases by choosing fixed small, intermediate or large values of δ_-, but simultaneously varying the rate δ_+. The results of our calculations and computer simulation predictions for the asymmetric dissociation rate are presented in figures 7–9.

When one of the dissociation rates is small ($\delta_- = 0.1$), varying the other dissociation rate strongly influences the phase diagram; see figure 7. Immediately as we reach $\delta_- \neq \delta_+$ the number of stationary phases increases to six. Two new phases, MC–LD/LD–LD and MC–HD/LD–LD, appear and grow in size because increasing the dissociation rate δ_+ allows for larger fluxes of positive particles to go through the system, while the fluxes of

https://doi.org/10.1088/1742-5468/abbed7

J. Stat. Mech. (2020) 113202

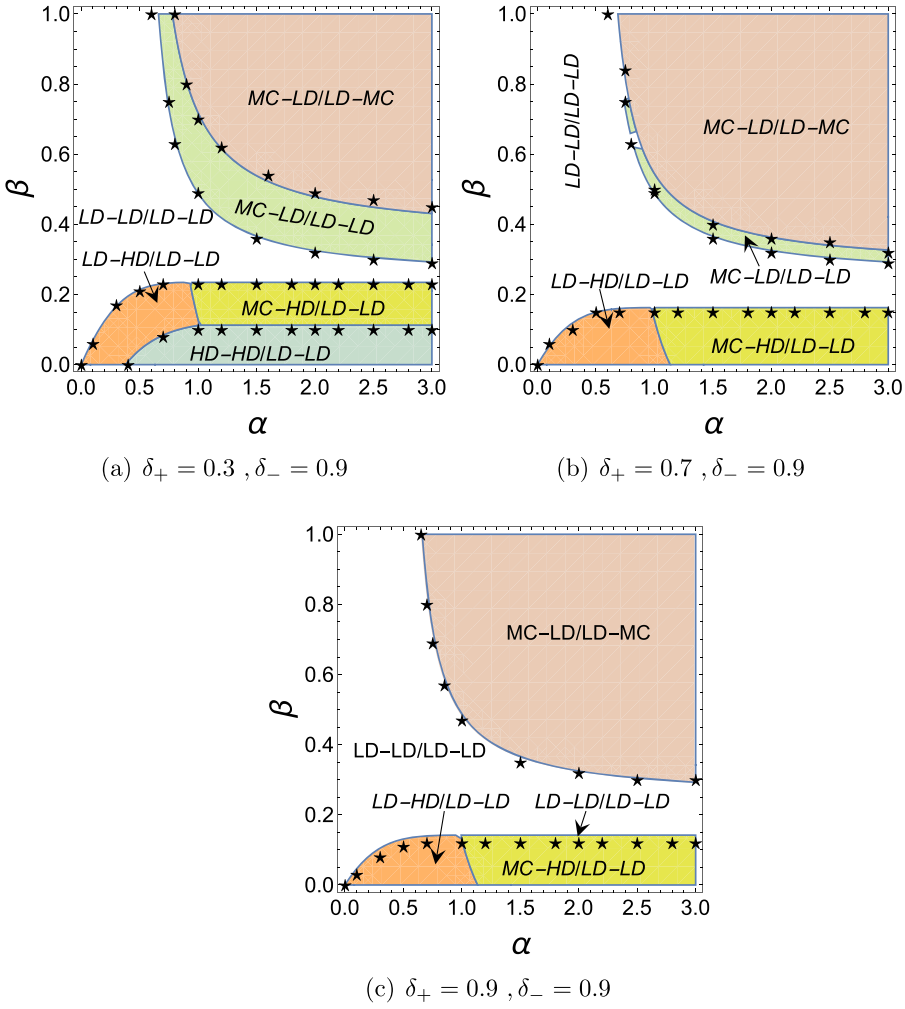

Figure 9. Stationary phase diagrams for increasing the dissociation rate δ_+ with the fixed dissociation rate $\delta_- = 0.9$. Solid lines are theoretical phase boundaries, while symbols represent the results from simulations.

negative particles do not increase. One symmetric phase, LD–LD/LD–LD, disappears because the symmetry conditions for the rates are not satisfied anymore.

We now focus on the properties of the system for varying values of δ_+ with the intermediate value $\delta_- = 0.5$. The results of theoretical calculations and computer simulations are illustrated in figure 8. Here the changes in the stationary phases are more complex. One can see that for $\delta_+ = 0.1 < \delta_-$, the same six asymmetric phases as discussed above can be in the system (figure 8(a)). Increasing δ_+ (from 0.1 to 0.5) leads to shrinking of the sizes of the HD–HD/LD–LD, MC–LD/LD–LD and MC–LD/LD–LD phases. Ultimately, when the rates are symmetric $\delta_+ = \delta_-$ only four phases are realized in the system as presented in figure 8(b). However, further increase in $\delta_+ > \delta_-$ changes the stationary phase diagram again: the phases MC–HD/LD–LD and MC–LD/LD–LD reappear and expand in size; see figure 8(b). As we argued above, the increase in the

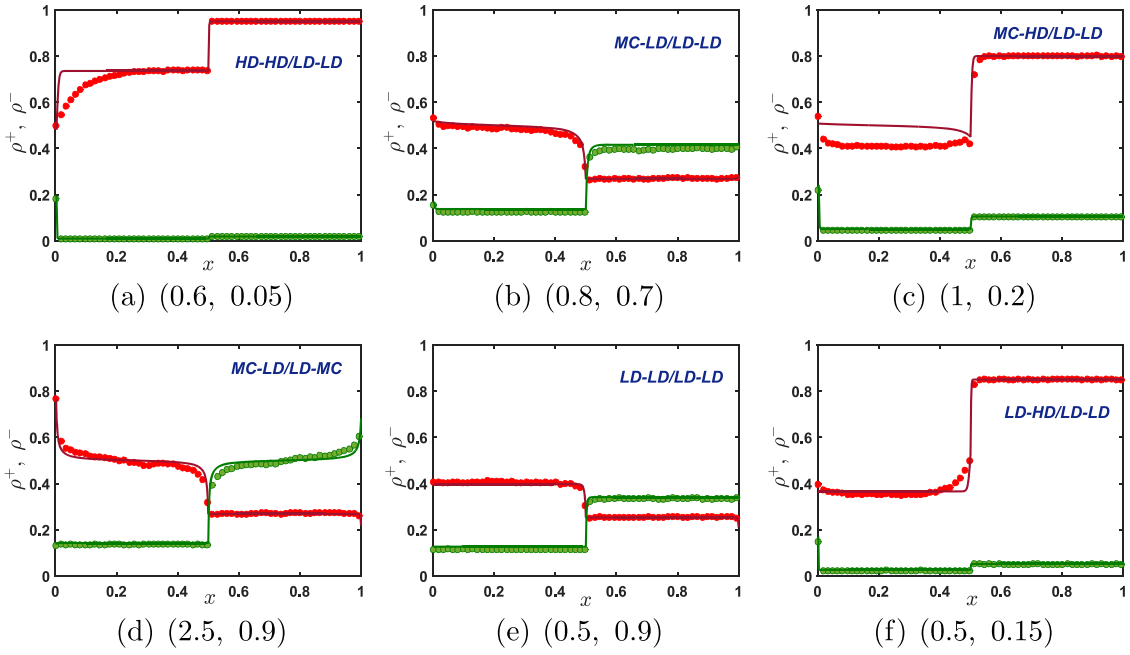

Figure 10. Density profiles for all possible stationary phases with the asymmetric dissociation rates $\delta_+ = 0.2$ and $\delta_- = 0.9$. The entry and exit rates (α, β) are specified in the sub-captions of the plots. Red and green symbols are the computer simulations results for the $(+)$ and $(-)$ particles, respectively. Correspondingly, the red and green solid lines are theoretical predictions.

dissociation rate δ_+ favors the appearance of the MC phases in the left sub-lattice for the $(+)$ particles.

The results presented in figure 9 show how the increasing values of the dissociation rate δ_+ with the fixed dissociation rate $\delta_- = 0.9$ modify the stationary behavior of the system. There are six phases in the system for $\delta_+ = 0.3$ (figure 9(a)), among which the HD–LD/LD–LD phase is the most sensitive to the increase in the dissociation rate. It vanishes for $\delta_+ > 0.5$ followed by a shrinkage in the size of the MC–LD/LD–LD phase and expansion of the MC–HD/LD–LD phase as described in figure 9(b). Eventually, for $\delta_+ = \delta_- = 0.9$ (figure 9(c)), the MC–LD/LD–LD phase completely disappears, but still five stationary phases, including two symmetric and three asymmetric phases, can be found in the system.

The density profiles for various stationary phases for the asymmetric dissociation rates are illustrated in figure 10. The theoretical results are generally in good agreement with computer simulations. Only a few deviations are found, suggesting that our theoretical method correctly captures the complex dynamics in the bidirectional transport of driven particles with local dissociations.

J. Stat. Mech. (2020) 113202

5. Summary and conclusions

To summarize, we investigated a theoretical model of bidirectional transport of driven diffusive particles along a 1D track when the particles are also allowed to dissociate irreversibly at special sites far away from the boundaries. It is stimulated by the motion of motor proteins moving in opposite directions along the cytoskeleton filaments. The model is formulated as the inhomogeneous version of the totally asymmetric simple exclusion process for two oppositely moving types of particles. Our theoretical method is based on the idea that local dissociations are viewed as a localized inhomogeneity that divides the system into two coupled homogeneous processes for which specific results are known. This allows us to develop a mean-field theoretical method to quantitatively describe non-equilibrium processes in the system. Our analytical calculations are also supported by extensive Monte Carlo computer simulations.

We specifically considered two different scenarios for the system dynamics: the symmetric case when dissociation rates for both types of particles are the same, and the asymmetric case when these rates are different. Introducing symmetric dissociation rates leads to significant changes in stationary phase diagrams depending on the amplitudes of these transitions. New dynamic regimes appear, some phases disappear, and other dynamic regimes expand or shrink. It is found that the SSB phenomena are still observed, and all dynamic phases are either symmetric or asymmetric. If the dissociation rates are not equal to each other (asymmetric scenario), the changes in the stationary phase diagrams are also significant with up to six total phases found in the system. But in this case all dynamic regimes are asymmetric. The exact number, dynamic properties and locations of different phases depend on specific values of all parameters in the system that include the entrance and exit transitions in addition to the dissociation rates. Simple physical arguments are presented to explain the theoretical observations.

Although our theoretical model captures some important features of the bidirectional transport of biological molecular motors, it is important to emphasize that it relies on several approximations. The main one is the assumption that dynamic processes in different sub-lattices do not affect each other. While this approach works reasonably well (as compared with computer simulation results), some deviations have been observed. In addition, many realistic properties of motor protein transport are not taken into account in our model. They include inhomogeneity in the translocation rates of different motors, the possibility of associations and dissociations along all parts of the filament, and many others. Incorporating such features into the existing model might help us to gain deeper insights into the diverse non-equilibrium systems persisting in nature.

Acknowledgments

A B K acknowledges the support from the Welch Foundation (Grant C-1559), from the NSF (Grant CHE-1953453) and from the Center for Theoretical Biological Physics sponsored by the NSF (Grant PHY-2019745).

J. Stat. Mech. (2020) 113202

References

[1] Alberts B, Johnson A, Lewis J, Raff M, Roberts K and Walter P 2007 *Molecular Biology of the Cell* (New York: Garland Science)
[2] Bray D 2000 *Cell Movements: From Molecules to Motility* (New York: Garland Science)
[3] Kolomeisky A B and Fisher M E 2007 *Annu. Rev. Phys. Chem.* **58** 675 –695
[4] Kolomeisky A B 2015 *Motor Proteins and Molecular Motors* (Boca Raton, FL: CRC Press)
[5] Fletcher D A and Mullins R D 2010 *Nature* **463** 485–492
[6] Schnitzer M J, Visscher K and Block S M 2000 *Nat. Cell Biol.* **2** 718–723
[7] Chowdhury D 2013 *Phys. Rep.* **529** 1–197
[8] Bressloff P C and Newby J M 2013 *Rev. Mod. Phys.* **85** 135
[9] McLaughlin R T, Diehl M R and Kolomeisky A B 2016 *Soft Matter* **12** 14–21
[10] Diehl T, Mallick K and Zia R K P 2011 *Rep. Prog. Phys.* **74** 116601
[11] Derrida B, Domany E and Mukamel D 1992 *J. Stat. Phys.* **69** 667–687
[12] Parmeggiani A, Franosch T and Frey E 2003 *Phys. Rev. Lett.* **90** 086601
[13] Krug J 1991 *Phys. Rev. Lett.* **67** 1882
[14] Popkov V, Evans M R and Mukamel D 2008 *J. Phys. A: Math. Theor.* **41** 432002
[15] Clincy M, Evans M R and Mukamel D 2001 *J. Phys. A: Math. Gen.* **34** 9923
[16] Leduc C, Padberg-Gehle K, Varga V, Helbing D, Diez S and Howard J 2012 *Proc. Natl Acad. Sci.* **109** 6100–5
[17] MacDonald C T, Gibbs J H and Pipkin A C 1968 *Biopolym.* **6** 1–25
[18] Derrida B 1998 *Phys. Rep.* **301** 65–83
[19] Popkov V, Rákos A, Willmann R D, Kolomeisky A B and Schütz G M 2003 *Phys. Rev.* E **67** 066117
[20] Evans M R, Juhász R and Santen L 2003 *Phys. Rev.* E **68** 026117
[21] Juhász R and Santen L 2004 *J. Phys. A: Math. Gen.* **37** 3933
[22] Nishinari K, Okada Y, Schadschneider A and Chowdhury D 2005 *Phys. Rev. Lett.* **95** 118101
[23] Evans M R, Foster D P, Godrèche C and Mukamel D 1995 *J. Stat. Phys.* **80** 69–102
[24] Krug J 2000 *Braz. J. Phys.* **30** 97–104
[25] Popkov V and Peschel I 2001 *Phys. Rev.* E **64** 026126
[26] Pronina E and Kolomeisky A B 2007 *J. Phys. A: Math. Theor.* **40** 2275
[27] Sharma N and Gupta A K 2017 *J. Stat. Mech.* 043211
[28] Evans M R, Foster D P, Godrèche C and Mukamel D 1995 *Phys. Rev. Lett.* **74** 208
[29] Klumpp S and Lipowsky R 2004 *Europhys. Lett.* **66** 90
[30] Jose R and Santen L 2020 *Phys. Rev. Lett.* **124** 198103
[31] Jose R, Arita C and Santen L 2020 *J. Stat. Mech.* 033207
[32] Arndt P F, Heinzel T and Rittenberg V 1998 *J. Stat. Phys.* **90** 783–815
[33] Appert-Rolland C, Ebbinghaus M and Santen L 2015 *Phys. Rep.* **593** 1–59
[34] Mirin N and Kolomeisky A B 2003 *J. Stat. Phys.* **110** 811–823
[35] Gomes L, Midha T, Gupta A K and Kolomeisky A B 2019 *J. Phys. A: Math. Theor.* **52** 365001
[36] Xiao S, Liu M and Shang J 2012 *Mod. Phys. Lett.* B **26** 1150036
[37] Greulich P and Schadschneider A 2008 *J. Stat. Mech.* P04009

J. Stat. Mech. (2020) 113202